SCIENCE CHINA
Chemistry

•REVIEWS•

March 2024 Vol.67 No.3: 774–787
https://doi.org/10.1007/s11426-023-1815-9

Lighting up plants with near-infrared fluorescence probes

Yida Pang[1,2†], Mengjiao Lu[1†], Hyeonji Rha[3†], Wenchao Yang[1*], Amit Sharma[4*], Yao Sun[2*] & Jong Seung Kim[3,5*]

[1]*National Key Laboratory of Green Pesticide, Key Laboratory of Green Pesticide and Agricultural Bioengineering, Ministry of Education, Center for R&D of Fine Chemicals of Guizhou University, Guiyang 550025, China;*
[2]*National Key Laboratory of Green Pesticide, College of Chemistry, Central China Normal University, Wuhan 430079, China;*
[3]*Department of Chemistry, Korea University, Seoul 02841, Korea;*
[4]*CSIR-Central Scientific Instruments Organisation, Sector-30C, Chandigarh, 160030, India;*
[5]*TheranoChem Incorporation, Seongbuk-gu, Seoul, 02856, Korea*

Received August 30, 2023; accepted September 18, 2023; published online October 23, 2023

Fluorescence imaging is a non-invasive and highly sensitive bioimaging technique that has shown remarkable strides in plant science. It enables real-time monitoring and analysis of biological and pathological processes in plants by labeling specific molecular or cellular structures with fluorescent probes. However, tissue scattering and phytochrome interference have been obstacles for conventional fluorescence imaging of plants in the ultraviolet and visible spectrum, resulting in unsatisfactory imaging quality. Fortunately, advances in near-infrared (NIR) fluorescence imaging technology (650–900 nm) offer superior spatial-temporal resolution and reduced tissue scattering, which is sure to improve plant imaging quality. In this review, we summarize recent progress in the development of NIR fluorescence imaging probes and their applications for *in vivo* plant imaging and the identification of plant-related biomolecules. We hope this review provides a new perspective for plant science research and highlights NIR fluorescence imaging as a powerful tool for analyzing plant physiology, adaptive mechanisms, and coping with environmental stress in the near future.

NIR fluorescent probe, plant, imaging, biologic application

Citation: Pang Y, Lu M, Rha H, Yang W, Sharma A, Sun Y, Kim JS. Lighting up plants with near-infrared fluorescence probes. *Sci China Chem*, 2024, 67: 774–787, https://doi.org/10.1007/s11426-023-1815-9

1 Introduction

The global population has already surpassed the 7.6 billion mark, with projections estimating a staggering increase to 9.2 billion by 2050. To meet the nutritional needs of the world's population, this escalation is predicted to trigger a corresponding rise in the demand for food worldwide, which is expected to increase by roughly 59%–102% [1–3]. Therefore, understanding the physiological state and health of plants is critical for increasing crop yields, enhancing ecosystem health, and safeguarding human food security.

Plant stress encompasses a range of adverse environmental circumstances that hinder plant growth, such as nutrient deficiency, water scarcity, inundation, temperature fluctuations, air pollution, and pests and diseases [4,5]. The prevailing methodologies for detecting plant stress can be categorized into three categories: molecular techniques, spectral analyses, and imaging modalities.

Molecular methods, such as polymerase chain reaction (PCR) and enzyme-linked immunosorbent assay (ELISA), can detect specific DNA or RNA sequences of plant pathogens. However, these methods require sophisticated labora-

†These authors contributed equally to this work.
*Corresponding authors (email: amitorg83@gmail.com; wcyang@gzu.edu.cn; sunyaogbasp@ccnu.edu.cn; jongskim@korea.ac.kr)

tory equipment and complex molecular biology techniques, making them relatively cumbersome and time-consuming to operate [6–9]. Spectroscopic methods detect pathogens by measuring the spectral signature of plant tissue. Although this approach is non-destructive and real-time, it is more susceptible to the effects of environmental factors, including light and the plant itself [10–12]. Infrared thermal imaging can detect temperature changes in plants, but it is greatly affected by environmental conditions and external factors [13]. Hyperspectral imaging can provide rich spectral information, but the technology is expensive, and the data processing is complex [14]. While these approaches have promise, they also have limitations in their capacity to be applied to the *in-situ*, real-time detection and analysis of biological samples due to their complexity and susceptibility to environmental factors.

Over the past few decades, fluorescence imaging has gained growing significance owing to its adaptability, high sensitivity, and capacity for *in situ* detection in real samples. It has permeated diverse fields, encompassing life sciences [15], drug exploration [16], and biomedical engineering [17], among others. Currently, a plethora of functional organic small molecules, fluorescent proteins, and inorganic nanomaterials have materialized, ushering in an era of plant imaging and detection.

These innovations serve diverse roles, such as monitoring plant hormones [18], signaling molecules [19], and ion concentrations [20], thereby affording insights into the intricate regulatory mechanisms underpinning plant metabolic pathways. However, most existing fluorescent probes utilized for plant imaging predominantly operate in the visible light range. This limitation often leads to challenges such as poor signal-to-noise ratio, heightened background fluorescence, and restricted tissue penetration, ultimately culminating in compromised imaging quality.

Fortunately, when fluorescent probes with near-infrared (NIR) windows are employed for plant imaging, they offer distinct advantages such as improved transparency, reduced tissue absorption and scattering, and minimized interference from spontaneous fluorescence. These advantages undoubtedly contribute to an enhanced quality of plant imaging [21–23]. In consequence, NIR probes hold the potential to realize deep tissue imaging within plants, providing more precise and quantitative data.

This review places a specific emphasis on elucidating the design principles, synthesis methodologies, and plant applications of NIR probes of varying types, including organic small molecules and inorganic nanomaterials. Then, a summary of their applications in plant imaging and detection of plant active molecules (reactive species, metal ions, signal molecules, *etc*.) follows. Additionally, the concluding section of this review offers a prospective outlook on the future developments and potential applications of NIR imaging agents in the context of plants.

2 Near-infrared fluorescence imaging of plants

Through the advanced technique of imaging plant cells, tissues, organs, and the entirety of plant bodies, we gain profound insights into the intricate physiological and biochemical processes governing plant life [24–27]. However, the presence of plant pigments like carotenoids (380–520 nm), anthocyanins (560–650 nm), and chlorophyll (600–700 nm) poses difficulties for traditional fluorescence imaging, which in turn reduces imaging contrast and accuracy [28]. To surmount this limitation, the application of long-wavelength fluorescence imaging reagents proves indispensable, as they effectively mitigate the interference of plant pigments, thereby elevating the clarity and resolution of fluorescence imaging. With powerful tools to examine and analyze the underlying complexities of plant physiology, adaptation mechanisms, and responses to environmental stimuli, this novel approach advances plant science and agricultural research.

2.1 Plant cell-level imaging

In plant cells, the lipid droplet is a type of dispersed suborganelle that not only stores energy but also participates in the lipid transport and metabolism regulation [29]. In general, the presence of both donor (D) and acceptor (A) groups in a dye molecule can facilitate intramolecular charge transfer (ICT) towards the near-infrared region. In the ICT mechanism, π-electrons transfer from the donor moiety of a molecule along the conjugated system to the acceptor moiety. By extending the π-conjugation and/or enhancing the donor-acceptor effect, Liu's team [30] successfully synthesized three imaging reagents with a narrow band gap and bright NIR emission. These reagents can effectively illuminate lipid droplets in oil-rich plant cells within the NIR region. The maximum emission wavelengths of compounds **1**, **2**, and **3** in toluene are observed at 664, 645, and 676 nm, respectively. In the solid state, they exhibited fluorescence quantum yields of 0.76%, 2.84%, and 0.70%, respectively. More importantly, excellent biocompatibility, remarkable photostability, and significant lipophilicity (Log*P* values for **1**, **2**, **3** are 9.39, 7.89, and 8.03, respectively) render these compounds highly suitable for application in organisms rich in lipid droplets. *In vitro* experiments revealed that these compounds had no significant cytotoxicity to tested HeLa cells and were mainly located in the lipid droplet of the cells (Pearson's coefficient values for **1**, **2**, **3** are 0.94, 0.96, 0.97, respectively). The bright NIR red fluorescence of **1**, **2**, and **3** in sunflower seed slices was observed by confocal fluorescence microscopy (Figure 1B).

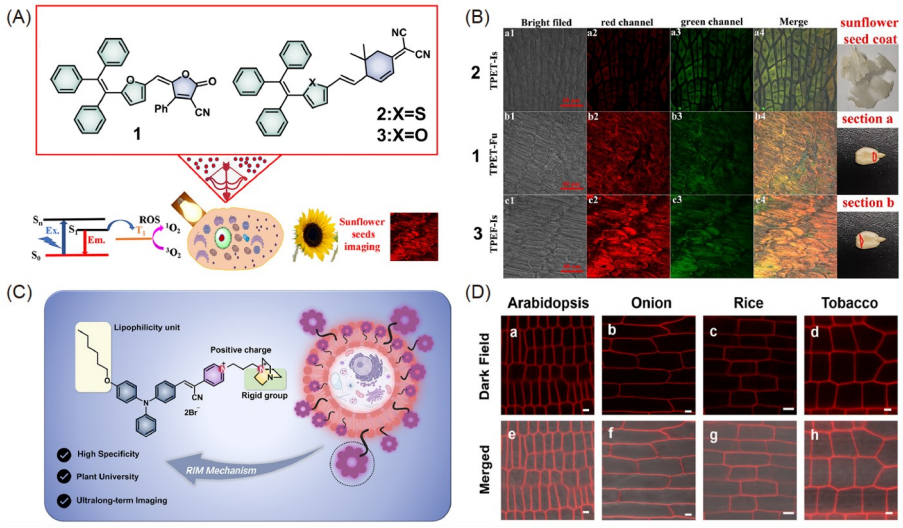

Figure 1 (A) The structure of compounds **1**–**3**. (B) Fluorescence imaging of sunflower seeds incubated with compounds **1**, **2**, **3**, and BODIPY493/503 Green. Scale bar: 60 μm. Reprinted with permission from Ref. [30]. Copyright 2022, Elsevier. (C) Schematic illustration of the design principle of compound **4**. (D) NIR fluorescence imaging of different plants with compound **4**. Scale bar = 5 mm (a, e), 50 mm (b, f), 10 mm (c, g), 5 mm (d, h). Reprinted with permission from Ref. [37]. Copyright 2023, Royal Society of Chemistry (color online).

As an essential component of cells, the plasma membrane plays a crucial role in segregating the internal and external cellular environment, and structural irregularities have been shown to be closely related with cell aging, apoptosis, and certain physiological disorders [31–35]. However, imaging the plasma membrane of plant cells is often constrained by aggregation-caused quenching (ACQ), limited imaging duration, and interference from the cell wall. Fortunately, the aggregation-induced emission (AIE) phenomenon, first discovered by the Tang's research group [36] in 2001, offers a promising solution to this problem. Specifically, AIE organic molecules exhibit minimal fluorescence in solution, but in the condensed state (when they form aggregates or a solid state), their luminescent properties are significantly enhanced due to restricted intramolecular motion (RIM) and the prevention of intramolecular π-π interactions.

Based on this, Qian's research group [37] devised and synthesized a water-soluble AIE type compound **4**. Compound **4** is composed of triphenylamine moiety as the propeller donor and α-cyanopyridine cation as the water-soluble acceptor. The presence of the rigid group, *i.e*, 4-diazabicyclo [2.2.2] octane in the side chain, effectively hindered the compound's penetration through the cell plasma membrane. In dimethyl sulfoxide (DMSO), probe **4** exhibited a maximum absorption at 525 nm in DMSO, with an absorption band encompassing the almost entire ultraviolet (UV)-visible region (300 to 660 nm). Experimental research revealed that probe **4** rapidly penetrated cell walls and selectively stained the plasma membranes of all plant cells in a very short time frame. This probe boasts advanced features, including ultrafast staining, excellent biocompatibility, and prolonged imaging capability (more than 10 h). Moreover, compared to commercially available FM dyes, the probe **4** showed exceptional plasma membrane specificity, eliminating the disturbance for staining other cellular regions. The mean signal-to-noise ratio of the plasma membrane in central cells and peripheral epidermal cells was measured to be about 106.3 and 144.4, respectively. Moreover, probe **4** delivered high-resolution fluorescence images of onion epidermal cells as well as root cells of Arabidopsis, rice, and tobacco seedlings, all with comparable resolution (Figure 1D). Collectively, observed results demonstrated the universal applicability of the probe **4** for staining various plant cell membranes.

2.2 Plant organ-level imaging

Rosenzweig's group [38] co-doped fluorenyl benzothiadiazole-derived polymers and maleic anhydride-derived polymers with NIR narrow emission skeleton chlorin to obtain semiconductor polymer dots **5**. The semiconductor polymer and fluorescent dye were successfully able to transfer fluorescence resonance energy, which allowed polymer dots **5** to outperform its predecessors in terms of photo-stabilization and brightness. The average hydrodynamic diameter of polymer dots **5** was measured to be 52 nm. The presence of free carboxylate groups on its surface allows for antibody modification and use in plant imaging applications. When excited by a laser at 450 nm, polymer dots **5** displayed an NIR emission band with an average full width at half maximum (FWHM) of just 25 nm. Cell experiments confirmed the good biocompatibility of prepared polymer dots. For imaging purposes, FLS_2 receptor-associated Arabidopsis, IgG (H + L) and F(ab) antibody fragments were further modified on the surface of polymer dots **5**. By using an

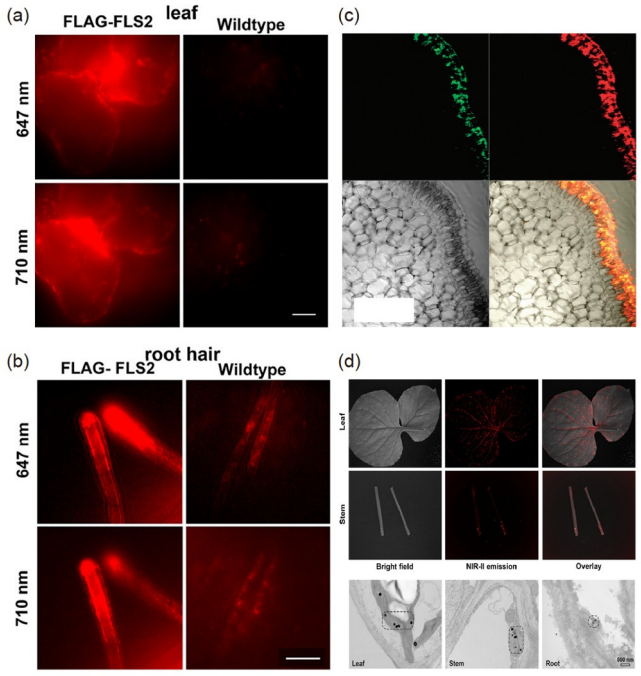

Figure 2 NIR fluorescence imaging of leaf cells (a) and root hair cells (b) incubated with polymer dots **5**. Scale bar = 50 μm. Reprinted with permission from Ref. [37]. Copyright 2022, American Chemical Society. (c) Fluorescence imaging of *Phalaenopsis* incubated with nanoparticles **6**. Scale bar: 50 μm. Reprinted with permission from Ref. [41]. Copyright 2009, American Scientific Publishers. (d) NIR-II imaging photographs of leaves and stems obtained from *N. benthamiana*, sprayed with nanoparticles **7** solution. Reprinted with permission from Ref. [42]. Copyright 2023, Royal Society of Chemistry (color online).

inverted microscope, **5** demonstrated imaging of leaf and root hair cells of *Arabidopsis thaliana* in NIR channels (647 and 710 nm) (Figure 2a, b). Furthermore, the blinking behavior of polymer dots **5** also suggested its potential for use in super-resolution imaging applications.

In general, lanthanides doped nanoparticles (Yb^{3+}/Er^{3+} or Yb^{3+}/Tm^{3+}, *etc*.) exhibit high photo-stabilization and quantum yields, making them excellent for real-time imaging over extended periods [39–41]. In this regards, Haase's research group [42] reported water-soluble up-conversion nanoparticles **6** ($NaYF_4$: 20% Yb, 2% Er), and demonstrated its imaging applications in *Phalaenopsis* and *Arabidopsis*. The modification of nanoparticles **6** with 1-hydroxyethane-1,1-diphosphonic acid resulted in the formation of a stable colloidal solution with an average diameter of 45 nm in water. Due to the co-doping with lanthanide metals, nanoparticles **6** exhibited dual emission at 550 and 660 nm under the excitation of a 974 nm laser. After adding the colloidal solution containing the nanoparticles **6** to the Phalaenopsis and Arabidopsis plants, confocal laser scanning microscopy was employed to capture the luminescence of the particles in the plant. The results showed that nanoparticles were readily absorbed by both the tested plants. Further, **6** may be ingested through the roots, transported along the flower stem to the leaves, and even dispersed throughout the entire plant. Notably, glowing particles were seen along the flower stalks of *Phalaenopsis* and *Arabidopsis* plants at heights of up to 10 and 4 cm, respectively. Additionally, the nanoparticles **6** showed a low plant autofluorescence background and clearly illuminated the blood vessels in the roots of *Phalaenopsis* (Figure 2c).

In 2023, Xu *et al*. [43] synthesized Ce^{3+}-doped shell-coated $NaErF_4$ nanoparticles (**7**) capable of dual-mode NIR up-conversion and NIR-II down-conversion emission. By modulating the energy capture center with Tm^{3+} ions and employing an appropriate Ce^{3+} doping concentration in the shell layer, the initial weak NIR-II emission peak (1,525 nm) of the core nanoparticles was greatly improved. This resulted in a remarkable 19-fold increase in the NIR-II luminescence properties of the nanoparticles **7**. The improvement allowed for both deep tissue penetration and a high SNR for subsequent plant optical bioimaging. Additionally, nanoparticles **7** were coated with polyethyleneimine to increase their water solubility and facilitate better plant uptake. Ultimately, these superior attributes of nanoparticles **7** facilitated successful NIR-II imaging of the *Nicotiana benthamiana* leaves and stems (Figure 2d). This study offers a fresh perspective for examining the uptake and trafficking of nanoparticles inside plant systems by introducing a unique plant imaging technique that makes use of NIR-II channels.

3 Near-infrared fluorescence detection of plant-related active molecules

The remarkable specificity and sensitivity of fluorescent probes are fundamental advantages in botanical investigations. By customizing these probes to target specific bioactive molecules in plants, such as reactive species, metal ions, signaling molecules, and harmful substances, precise and quantitative detection of these pivotal active molecules can be achieved. These active molecules assume pivotal regulatory functions in the intricate processes of plant growth, development, stress responsiveness, and acclimatization to dynamic environmental fluctuations [44–49].

3.1 Reactive species and signal molecule

In the context of plant growth, reactive oxygen species (ROS) and reactive sulfur substances (RSS) are crucial redox molecules. These molecules demonstrate a dual function in the physiological regulation of plants. Controlled ROS and RSS levels act as signaling molecules, participating in stress responses, orchestrating growth, disease resistance mechanisms, and maintaining intracellular redox homeostasis. Nonetheless, an excessive accumulation of these active substances may cause oxidative damage, instigating lipid

peroxidation of cell membranes and protein impairment, which would disrupt normal cell metabolism [50–52].

Hydrogen sulfide, a multifunctional regulator of plant growth and development, is essential for germination, root organogenesis, cell senescence, and autophagy, among other stages of the plant life cycle. Moreover, hydrogen sulfide enhances the plant's resilience against adversities such as ion imbalances and drought [53–55]. The 2,4-dinitrophenyl ether group, as a strong electron-withdrawing group, affects the electron density of the probe molecule through its interaction with the fluorophore, thereby triggering photo-induced electron transfer (PET), leading to the quenching of the dye's fluorescence. Nucleophilic reagent H_2S can react with the 2,4-dinitrophenyl group, causing its departure and accompanied by the restoration of the dye's luminescent properties. Wu's research group [56] designed a D-A type small molecular probe **8**, incorporating a hemocyanin-based modular scaffold as the electron acceptor and a xanthene derivative as the donor. Through the cleavage of the dinitrophenyl ether group, this molecule can precisely recognize H_2S in physiological environments.

With water-soluble groups present in its structure, spectral data acquired in DMSO/phosphate buffer saline (PBS) (*V*/*V* = 5:95) revealed that probe **8** exhibited a maximum absorption peak at 575 nm and a broad emission band ranging from 650 to 850 nm. Upon incubation with NaSH (50 mM), the absorption bands of probe **8** at 575 nm diminished, while those at 632 and 685 nm gradually intensified, leading to an isoabsorptive point at about 600 nm (Figure 3b). The mechanism by which probe **8** responded to H_2S may involve the detachment of the dinitrophenyl ether group, leading to the cessation of the PET process and the change of the ICT process. Concurrently, the fluorescence of probe **8** underwent significant enhancement, with a response time of approximately 30 min. Probe **8** exhibited remarkable resilience against interference during H_2S detection, including various tested common metal ions and anions (Figure 3c). Additionally, probe **8** also demonstrated excellent sensitivity in recognizing H_2S (0.75 μM). The exceptional performance of **8** was demonstrated in imaging Al^{3+}-induced abnormalities in H_2S content during early wheat germination (Figure 3d).

Likewise, by utilizing the 2,4-dinitrophenyl ether group as the leaving group and conjugating it with the xanthene-based benzothiazole derivative, probe **9** was developed for *in-situ* imaging of H_2S content in rice (Figure 3e) through the "Turn On" mechanism of ICT [57]. With a remarkable low detection limit of 104 nM, probe **9** showed a quick and highly selective reaction to H_2S. Upon the addition of H_2S, its emission wavelength at 720 nm experienced "Turn On" enhancement.

The Chen research group [58] also developed a water-soluble NIR H_2S "Turn On" small molecular based probe **10**, that exhibits exceptional selectivity and high sensitivity to H_2S within the physiological environment of plants (limit of detection (LOD) = 0.21 μM). Interestingly, probe **10** was employed for direct *in-situ* imaging of H_2S in rice roots (Figure 3f), which showed an upregulation of the H_2S signaling pathway under conditions of Al^{3+} exposure and

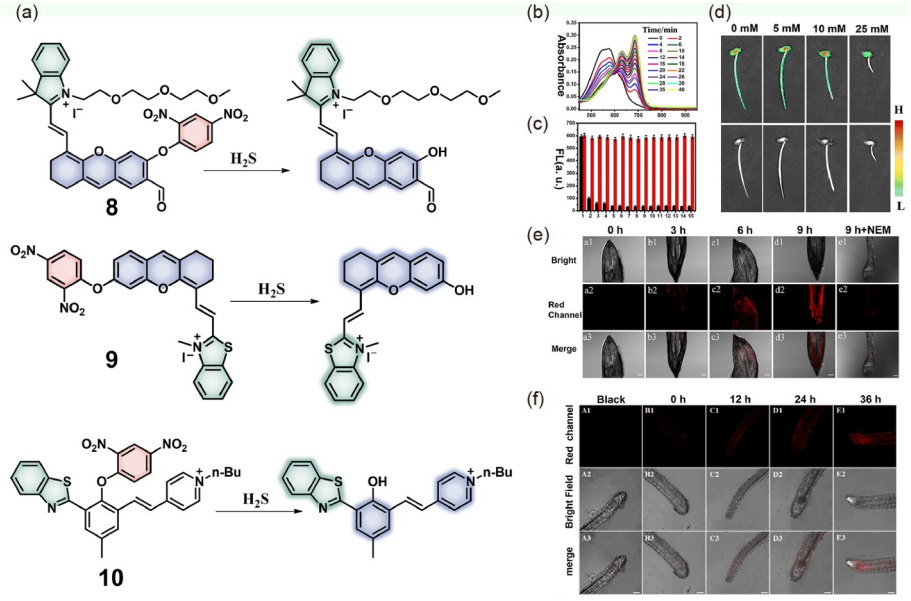

Figure 3 (a) The structures of probes **8**–**10**. (b) Change in the absorption spectra of probe **8** on incubation with NaSH in solution. (c) The selectivity of compound **8** for NaSH in solution. (d) Fluorescence images of compound **8** for wheat seedlings exposed to different concentrations of Al^{3+} ions. Reprinted with permission from Ref. [56]. Copyright 2023, Royal Society of Chemistry. (e) Fluorescence imaging of endogenous H_2S in rice roots using compound **9**. Scale bars = 100 μm. Reprinted with permission from Ref. [57]. Copyright 2023, American Chemical Society. (f) Fluorescence imaging of endogenous H_2S in rice roots using **10**. Scale bar = 25 μm. Reprinted with permission from Ref. [58]. Copyright 2021, American Chemical Society (color online).

flooding stress. These studies provide an effective detection tool to investigate the physiological and pathological roles of H_2S in plants.

Numerous environmental variables, including pathogen infection, high temperature, salt, injury, and light stress have been found to cause excessive H_2O_2 production in plants [59–61]. Wu *et al*. [62] meticulously designed and synthesized a NIR fluorescence probe **11**, with a diphenylamineyl xanthrene group and bis(methylenemalononitrile)indan as an electron donor and acceptor, respectively (Figure 4a). In plant physiological environment, it can accurately and efficiently react with H_2O_2 through the phenylboronic acid group serving as the recognition site. Probe **11** showed considerable AIE behavior in water/acetonitrile mixtures with various volume ratios. When the acetonitrile content reached about 20%, the relative quantum yield of the probe was measured as 0.37%. By encapsulating probe **11** with DSPE-PEG2000, nanoparticles having a hydrodynamic diameter of 109.5 nm were produced in order to improve biocompatibility. Under 808 nm excitation, nanoparticles **11** showed a maximum emission peak at 925 nm in water. In response to H_2O_2, nanoparticles **11** exhibited remarkable selectivity and robust anti-interference capability.

Studies have shown that toxic Cd^{2+} entering plants through the water/soil, where crops are grown, causes abnormal H_2O_2 content in plants, and thereby restrict or stop the plant growth. In this regard, the nanoparticles **11** were used to image okra sprouts/seedlings induced by Cd^{2+} exposure at different periods. The fluorescence signals of the okra sprouts/seedlings were clearly visible, and the NIR fluorescence signals increased with the increase of the Cd^{2+} level.

Interestingly, in the same year, the research group also reported another NIR-II fluorescence "Turn On" type probe **12** for the detection of H_2O_2 levels [63]. By using phenylboronic acid pinacol ester as the recognition site, H_2O_2 can lead to fluorescence enhancement of probe **12** at 1,036 nm (Figure 4b). AIE feature of probe **12** ensures strong fluorescence in the aggregated state of NIR-II imaging in aquatic environments. Probe **12** was successfully demonstrated to study and detect biomarker-activated H_2O_2 abnormalities in plant buds caused by various environmental stresses such as Cd^{2+} or high salt (NaCl) exposure in bean

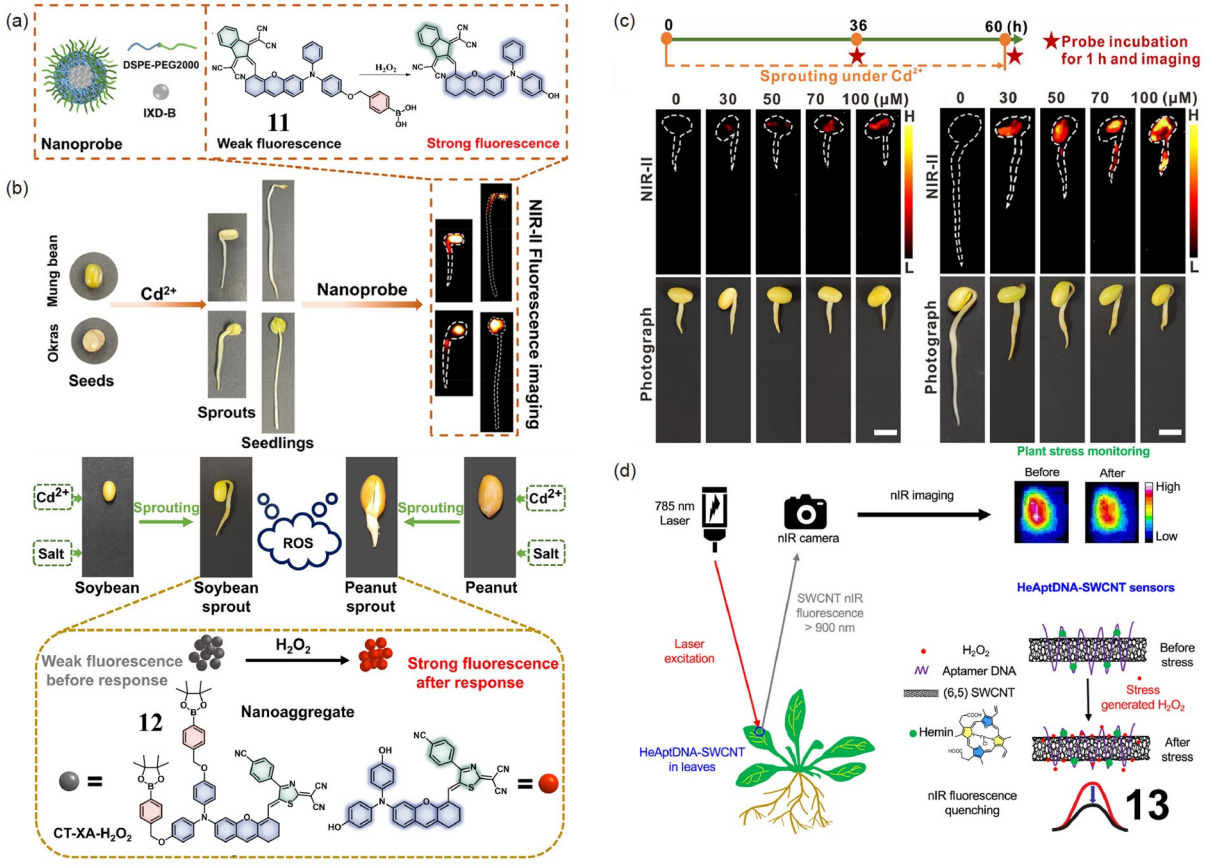

Figure 4 (a) Schematic illustration of the design principle of polymer dots **11** and its imaging application in bean sprouts. Reproduced with permission from Ref. [62]. Copyright 2022, American Chemical Society. (b) The schematic diagram for the fluorescence imaging of compound **12** under different oxidative stress conditions. (c) Photographs and fluorescent images of soybean sprouts coming from the sprouting process in water containing Cd^{2+} for 36 or 60 h. Scale bar: 1 cm. Reprinted with permission from Ref. [63]. Copyright 2022, Wiley. (d) Scheme depiction of nanosensor **13** preparation and *in vivo* monitoring of plant health. Reprinted with permission from Ref. [65]. Copyright 2020, American Chemical Society (color online).

sprouts (Figure 4c).

As a quasi-one-dimensional quantum wire, single-walled carbon nanotubes (SWNTs) have many unique inherent physical and chemical properties, such as low bandgap, large stoker shift, and excellent photostability, thus are ideal candidates for plant imaging [64]. Giraldo *et al*. [65] reported a nanosensor **13**, composed of SWNTs as the NIR imaging component, wrapped with a layer of DNA aptamer sequence and hemin through non-covalent bond interaction, to realize highly sensitive and highly specific recognition of hydrogen peroxide in the plant (Figure 4d). The nanosensor **13** displayed a strong absorption band covering 800 to 1,200 nm in the PBS or TES buffer solution, with a broad emission band with a main peak at 991 nm. The hemin in the nanosensor effectively catalyzes H_2O_2 to generate the active hydroxyl radical, quenching its fluorescence emission in a manner similar to the protonation reaction. The nanosensor **13**'s response to H_2O_2 was unaffected by the presence of Ca^{2+}, sucrose, glucose, methyl salicylate, or any other of these substances. Additionally, nanosensor **13** exhibits good biocompatibility when incubated with plant leaf cells. Under the 785 nm laser excitation, nanosensor **13** fluorescence quenching (14%) was observed in plant leaves exposed to H_2O_2. Given its great sensitivity, this nanosensor can respond to H_2O_2 in the plant's physiological range (10–100 μM). Hence, it may be used to achieve real-time observation and quantitative analysis of the molecular and biological processes inside living plants, thus providing a new tool for plants to prevent plant diseases at an early stage.

The dysregulation of plant signaling molecules, including phytohormones, ethylene, and nitric oxide (NO), serves as a pivotal parameter for real-time monitoring of plant health. For instance, diverse hormone types can intricately interact through signal transduction networks to uphold plant homeostasis. Nevertheless, an overabundance of hormones may impair growth and development, manifesting as deformities or excessive elongation in plants [66,67].

An essential plant hormone called auxin coordinates crucial roles in plant growth and development. It governs cell division, elongation, and differentiation, influencing the maturation of roots, stems, leaves, and pivotal processes like flowering and fruit formation. Auxin's reach extends to photosynthesis, root expansion, nutrient transport, and an array of physiological functions. Skillful auxin regulation augments crop yield elevates quality, and plant resilience to environmental stresses. However, an excess or deficiency of auxin can lead to aberrant plant growth, with cascading effects on yield and quality. In 2021, Strano *et al*. [68] synthesized two types of cationic polymer coated SWNTs-based nanosensors **14** and **15**. One end of the polymers was linked to a planar aromatic system for π-π stacking adsorption, while the other end was connected to hydrophilic cationic side chains, facilitating selective auxin recognition in solution. The results showed that the fluorenyl benzene- and imidazole-modified nanosensors **14** and **15** can achieve highly selective and specific recognition of 1-naphthaleneacetic acid (NAA) (8.2 μM) and 2,4-dichlorophenoxyacetic acid (2,4-D) (0.35 μM), respectively. Nanosensors **14** and **15** demonstrated remarkable photostability and superb NIR emission properties. Under continuous 785 nm laser excitation, sensors **14** and **15** were utilized to capture the spatiotemporal distribution of 1-naphthaleneacetic acid and 2,4-dichlorophenoxyacetic acid in spinach leaves at various time points (Figure 5a). In 2023, the same research group used a similar methodology to modify SWNTs with styrene-derived polymers containing sulfonate groups and ammonium ions and successfully achieved high selectivity and sensitivity in the recognition of two distinct gibberellins (GA_3 and GA_4) in the NIR window [69].

Endogenous nitric oxide (NO) holds significant physiological importance across various organisms. It acts as a signaling molecule at every step of the plant lifecycle and plays a significant role in plant pathology, serving as a major regulatory component in plant development and morphogenesis. Wu *et al*. [70] reported a water soluble nanosensor **16** for detecting NO within plants through the self-assembly of rotor-type naphthyl diphenylamine-based small molecule with cyclodextrin. The AIE properties of the small molecule were validated in a glycerol/water mixture (containing 1% DMSO), where the fluorescence intensity of the small molecule increased with the increasing proportion of glycerol in the system. In an aqueous solution, the small molecule formed stable nanoparticles with β-CD, exhibiting a hydrodynamic diameter of 105 nm. The prepared nanoparticles showed remarkable photostability. The addition of NO gradually increased the photoacoustic signal at 680–900 nm as well as the nanosensor **16**'s fluorescence signal at 938 nm. It is noteworthy that researchers utilized nanosensor **16** to achieve clear fluorescence imaging of NO in soybean sprouts in the NIR region (Figure 5b).

3.2 Metal ion

As essential components of enzymes, metal ions play an irreplaceable and pivotal role in catalytic reactions, facilitating fundamental biochemical processes including redox and photosynthesis. These metal ions also actively participate in signal transduction and hormone regulation, exerting significant impact on the plant stress response [71,72]. However, few NIR probes for metal ion detection in plants have been reported up to now. Cyanine derivatives are a significant class of water-soluble long-wavelength dyes, offering the potential for easy wavelength adjustment to NIR-Ia and even NIR-II regions [73–75]. In this regard, Lin *et al*. [76] designed a cyanine-based probe **17** that introduced an

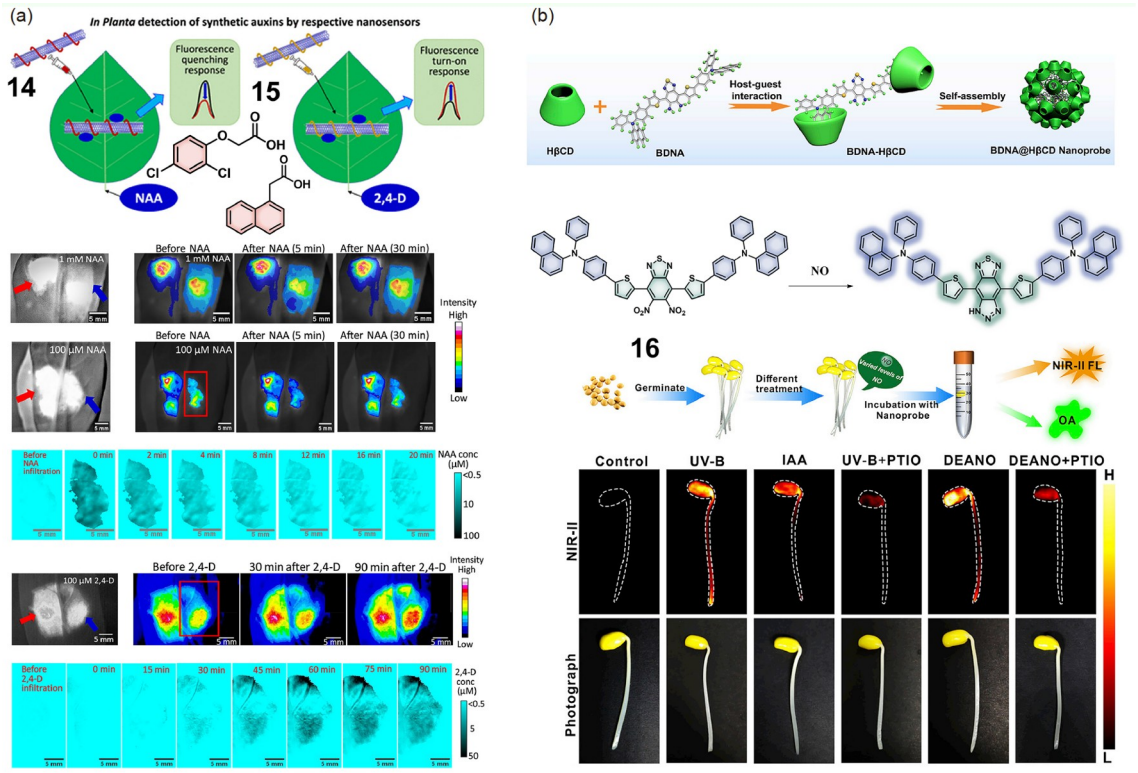

Figure 5 (a) Schematic illustration of nanosensors **14** and **15** for sensing NAA and 2,4-D in a spinach leaf. Reproduced with permission from Ref. [68]. Copyright 2021, American Chemical Society. (b) The preparation process and NO response mechanism of compound **16**, and its fluorescence imaging in bean sprouts. Reproduced with permission from Ref. [70]. Copyright 2022, Elsevier (color online).

amino-linked polypyridine structure at its *meso* site for efficient imaging of Cu^{2+} in aqueous solutions. This is a "PET" type probe based on nitrogen atom's lone pair electrons to quench cyanine fluorescence. When the probe is exposed to an aqueous solution containing Cu^{2+}, the polypyridine structure can strongly chelate the Cu^{2+}, which "Turn On" the NIR photoacoustic signal. The probe was further used to image copper ions in soybean sprouts. After the probe interaction with Cu^{2+}, the original absorbance band at 625 nm disappeared, and a new absorption band appeared at 715 nm, which was enhanced with the increase of copper ion concentration. Probe **17** exhibited an excellent selectivity and sensitivity (10.8 nM) to Cu^{2+} in the physiological environment. *In vivo* experiments have shown that after the soybean sprouts were pretreated with Cu^{2+}, the intensity of the photoacoustic signal of probe **17** was 2.06 times higher than that of the original photoacoustic signal. This strategy offers fresh insights for the subsequent realization of highly sensitive, highly selective environmental monitoring and non-invasive disease diagnosis with high imaging depth (about 10 cm).

Hg^{2+} endangers plant growth by impairing the growth of the roots and leaves. They interfere with photosynthesis, inhibit nitrogen metabolism and protein synthesis, resulting in leaf yellowing and wilting as well as reduced yield, and quality. Furthermore, Hg^{2+} can accumulate within plants and be transferred to humans through the food chain, posing a threat to human health. Yin's research group [77] reported an NIR BODIPY-based probe **18** to effectively detect Hg^{2+} in a physiological environment through a macrocyclic thioether as the recognition unit. Upon the addition of Hg^{2+}, the absorption bands of probe **18** at 580 to 820 nm gradually disappears, while those at 670 nm become significantly enhanced, resulting in an isoabsorptive point at around 701 nm. This is accompanied by change in color of probe solution from light brown to green. This alteration takes place because the PET effect from the macrocyclic thioether to the BODIPY core is severely hampered by the addition of Hg^{2+}. The Job's curve showed that the chelate ratio of probe **18** with Hg^{2+} was 1:1, with a binding constant K_a of 6.4×10^4 m^{-1}. The probe exhibited high selectivity for Hg^{2+} among other tested cations. More importantly, probe **18** demonstrated a very low detection limit for Hg^{2+} (2.66×10^{-4} mol/L). MTT assay demonstrated low cytotoxicity of probe **18** to HeLa cells and good biosafety in the concentration range from 2.5 to 100 μM. Through *in vivo* experiments, the distribution of Hg^{2+} in plant tissues was successfully imaged using an imaging channel of 640 nm and an exposure time of 120 ms (Figure 6b).

Corona-phase molecular recognition technology is an advanced method used to detect and identify specific molecules in plant cells and tissues. It utilizes a microfluidic chip and

the corona phase effect to concentrate the molecules in the sample and interact with a specific probe, resulting in the generation of a fluorescent signal. By analyzing the intensity and features of the fluorescence signal, the presence and concentration of the target molecule can be precisely determined [78]. This technology boasts high sensitivity, selectivity, and rapid response characteristics. Considering this, Strano's research group [79] developed a SWNTs-based nanosensor **19** containing single-stranded DNA decorative to detect arsenite in plants (Figure 6c). Based on the hydrogen bonds formed by guanine (G) and thymine (T) nucleotides with arsenite, nanosensor **19** can detect arsenite in plants with excellent selectivity. The presence of arsenite can significantly enhance the fluorescence intensity of the nanosensor, and its detection limit was found to be about 122 nM. The research showed that nanosensor **19** can be embedded in plant leaves to detect arsenite through the natural transpiration of plants. By irrigating the roots of spinach with a culture solution containing arsenite, the arsenite was transported throughout the body along the plant's blood vessels and subsequently detected in the leaves with nanosensor **19**. In addition, the sensing capability of the nanosensor **19** in rice and fern plants with strong arsenic ion tolerance was also verified. This new nanotechnology provides guidelines for future real-time monitoring of various indicators to be analyzed in plants in diverse environmental conditions.

3.3 Other substances

During the course of plant growth and development, various deleterious substances can induce plant intoxication, susceptibility to diseases, or exposure to adverse environmental conditions. These factors significantly impact how plants normally grow and develop, leading to a deceleration in their growth rate, decreased productivity, and, in extreme cases even causing plant death [80–82]. Appropriate concentrations of NaCl have a promoting effect on plant growth, as sodium ions stimulate cell expansion and water balance, thus fostering overall plant growth. However, in environments with high concentrations of sodium chloride, plant growth, and development are severely restricted due to decreased water potential, ion imbalance, and toxic effects [83–85].

Yang's research group [86] designed an NIR heptamethine cyanine probe **20** (Figure 7), which can detect sodium chloride in real time by forming J-aggregates through electrostatic interactions with NaCl. The absorption spectra showed that in an aqueous solution containing halide sodium ions, probe **20** displays absorption peaks at 770 and 862 nm, with the latter primarily attributed to the formation of J-aggregates. Likewise, the emission peak of probe **20** at 798 nm also decreases with an increase in sodium chloride content, exhibiting a noticeable blue shift. Probe **20** demonstrates a linear detection range for sodium chloride in aqueous solution up to 170 μM and exhibits rapid fluorescence response capability. Confocal microscopy images reveal that probe **20** is predominantly localized in the mitochondria of plant cells. Under non-saline stress conditions, both Arabidopsis root tip tissue imaging and whole-body imaging exhibit uniformly bright NIR emissions (Figure 8A). However, with increasing sodium chloride concentration, the observed fluorescence intensity gradually diminishes, while spermine effectively alleviates the plant's salt stress levels. This probe offers robust technical support for monitoring the extent of sodium chloride stress in plants.

The main effects of hydrazine on plants include cell

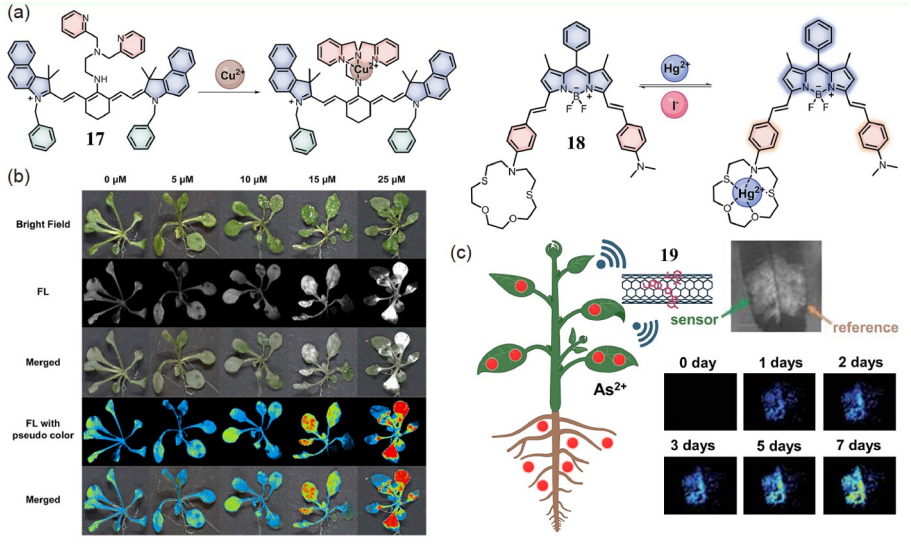

Figure 6 (a) The structure of compounds **17** and **18**. (b) The fluorescence images of Arabidopsis thaliana seedlings soaked with different concentrations of mercury ions of Hg^{2+} and compound **18**, respectively. Reproduced with permission from Ref. [77]. Copyright 2022, Elsevier. (c) Scheme depiction of nanosensor **19** in use of plants. Reprinted with permission from Ref. [79]. Copyright 2020, Wiley (color online).

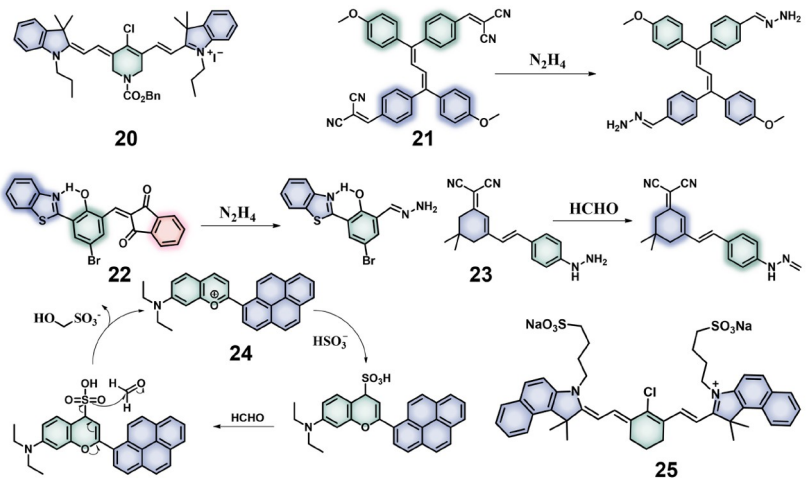

Figure 7 The structure of compounds **20**–**25** (color online).

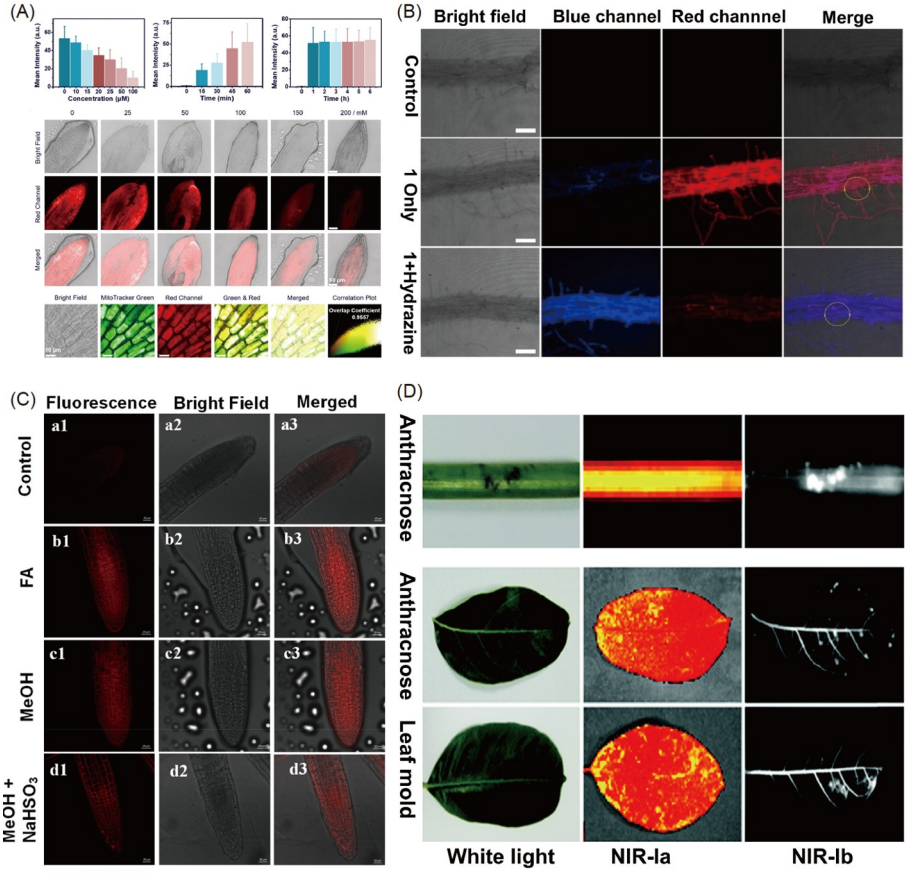

Figure 8 (A) Fluorescence imaging of compound **20** under NaCl stress in Arabidopsis thaliana. Scale bar = 10 μm. Reprinted with permission from Ref. [86]. Copyright 2023, Wiley. (B) Compound **21** for fluorescence imaging of hydrazine in root segments (mature region). Scale bar = 300 μm. Reprinted with permission from Ref. [88]. Copyright 2020, Elsevier. (C) Fluorescence imaging of Arabidopsis root tissue using compound **23** under different conditions. Scale bar = 20 μm. Reprinted with permission from Ref. [92]. Copyright 2023, Elsevier. (D) NIR-Ia and NIR-Ib images of the leaf and flower of *R. rugosa* under the use of compound **25**. Reprinted with permission from Ref. [94]. Copyright 2018, Royal Society of Chemistry (color online).

damage, interference with nutrient uptake and metabolism, suppression of growth and development, and detrimental effects on soil and ecosystems [87]. Hydrazine as a moderately strong nucleophilic reagent, contains two nitrogen atoms with lone pairs of electrons and four hydrogen atoms in its structure. It exhibits strong reducing properties, high

alkalinity, and good water solubility. Liu *et al*. [88] reported a novel red-emitting fluorescence probe **21**, containing a dicyanoethylene moiety for colorimetric and ratiometric detection of hydrazine, demonstrating good sensitivity (2.88 ppb). This probe was successfully employed for NIR imaging of fern roots (Figure 8B). Erdemir's research team [89] developed a ratio-type NIR fluorescence probe **22** based on the ICT "Turn Off" mechanism. Probe **22** exhibits high selectivity, good sensitivity (1.29 μM), and rapid response time (2.0 min). Notably, this probe was utilized for the localization of hydrazine in onion tissue through the red and green fluorescence channels.

Formaldehyde (FA) can lead to plants primarily manifests as growth inhibition, photosynthesis suppression, damage to leaf and cell structures, and disruption of nutrient absorption and metabolic processes. High concentrations of formaldehyde can also lead to leaf dehydration and wilting [90,91]. In response to this issue, Liu's research group [92] designed and synthesized an NIR fluorescence "Turn On" probe **23** based on the "PET off" mechanism for imaging formaldehyde in physiological environments. In comparison to the control group (1.8%), the fluorescence quantum yield of the probe in the presence of FA was observed to be 30%. Probe **23** exhibited good selectivity with a detection limit of 0.048 μM for FA. After inducing endogenous FA production in Arabidopsis root tissues with 10% methanol in PBS, the fluorescence intensity of the root tissue increased 4.9-fold as compared to the control group (Figure 8C). Furthermore, in 2022, Liu *et al*. [93] developed a novel NIR fluorescence probe **24** based on benzopyran and pyrene for cyclic detection of HSO_3^- and formaldehyde in live plant cells, with a detection limit for formaldehyde at 105 nM. Fluorescence confocal microscopy demonstrated that probe **24** can image trace amounts of formaldehyde in the mitochondria of live Paulownia root cells.

Cai *et al*. [94] synthesized a water-soluble, long-wavelength phthalocyanine derivative with imaging capabilities in the NIR-Ib region, enabling high-resolution visualization of water transport in plant growth, vascular systems, and early anthracnose infection sites. In an aqueous solution, the probe **25** exhibited a maximum absorption peak at 688 nm and broad emission bands centered at 815 and 950 nm. Fluorescence imaging demonstrated that the SBR of NIR-Ib images of red leaves and flowers of IR-820-labeled red roses was approximately 5-fold and 7-fold higher than NIR-Ia images, respectively. Furthermore, imaging of water movement in various plant states indicated that branches with larger leaves or greater leaf numbers exhibited more pronounced hydraulic channels. NIR-Ib fluorescence imaging was also performed on common plant fungi, anthracnose fungus, and fir fungus, revealing distinct bright spots and root nodule patches of varying shapes and sizes (Figure 8D).

4 Summary and outlook

Understanding molecular dynamics and biological mechanisms in living plants has become increasingly important for figuring out how plants grow and develop, regulate their metabolism, and react to stress as our understanding of plant biological processes has improved. In this review, we provide a concise overview of the implementation of NIR fluorescent probes in plant imaging and the detection of plant-associated active molecules, encompassing active compounds, metal ions, plant hormones, and harmful substances.

Fluorescent probes have emerged as a crucial and fruitful imaging technique following decades of advancement. Their utilization in the early identification of abiotic and biotic stress in plants provides insightful guidance. Nevertheless, certain inadequacies persist in the current fluorescence probe technology for plant physiological and pathological imaging.

Currently, the emission wavelength ranges of probes used in plant imaging mostly fall within the NIR region (650–900 nm). However, plant tissues are rich in pigments, and when used with exogenous fluorescent probes, their natural fluorescence may interfere with signals. For instance, the class of plant pigments known as chlorophyll, composed of porphyrin rings, also exhibits robust absorption and emission in the NIR region. The presence of chlorophyll may lead to substantial signal interference, weakening or completely absorbing the fluorescence intensity of the probe, ultimately reducing imaging sensitivity and signal-to-noise ratio [95–98]. Therefore, it is imperative to further redshift the maximum emission of the fluorescent probe into the second NIR region (1,000–1,700 nm). The light within this band possesses strong penetration capability, enabling it to reach deeper layers of plant tissues. Simultaneously, it is less influenced by the absorption of plant pigments, effectively minimizing pigment interference, and facilitating the acquisition of more precise and clear internal plant information [99–103].

The majority of conventional NIR plant fluorescent probes are organic compounds with extensive π-conjugated systems and limited water solubility. However, since most plant cells and tissues are found in aqueous environments, the presence of probes in these environments may cause fluorescence quenching. To produce better imaging results, the probe's water solubility must be increased, for example, by adding hydrophilic substitutes to the compound's structure, such as polyethylene glycol groups, sulfonic acid groups, and quaternary ammonium cation groups [104–106]. Water-soluble probes are more biocompatible and less harmful to biological samples, promoting plant health and growth. Additionally, water-soluble probes possess superior intracellular permeability, facilitating rapid and efficient interaction with target molecules within plant cells, thus yielding more precise

imaging results. Moreover, water-soluble probes possess improved *in vivo* diffusion, resulting in reduced non-specific background signals in tissues and cells, thereby enhancing the clarity and accuracy of the imaging process.

Currently, the majority of organic small molecules or inorganic nanoparticles utilized for detecting factors contributing to abnormal plant growth can only identify and report a single analyte in plants. However, the concentrations of these analytes fluctuate dynamically in plants, and they might even transform into other chemicals while being detected. Hence, researchers need to develop multi-channel probes to accomplish the task of detecting multiple indicators simultaneously at the same time and space [107–110]. These probes can concurrently detect various targets, such as pathogenic microorganisms, metabolites produced by pathogens, and disease resistance reaction substances in plants. This comprehensive approach facilitates a thorough understanding of disease development and pathological mechanisms, minimizing the chances of omissions and misdiagnoses.

Additionally, researchers should develop more imaging modalities for plant-related fields. For example, techniques such as photoacoustic imaging and Raman imaging offer great potential. Photoacoustic imaging combines the advantages of optics and acoustics, providing high-resolution deep tissue imaging, making it suitable for observing internal structures in plants like roots, stems, and leaves [111]. Raman imaging can be employed for chemical composition analysis, stress response studies, growth and development monitoring, and environmental adaptability research. Furthermore, conducting multimodal imaging can enhance the reliability of experimental results [112–116].

In summary, the primary objective for the future is the practical application of these NIR probes in agriculture. This necessitates conducting field trials to validate the probes' performance and providing training to farmers to ensure effective technology utilization. Moreover, establishing a data management system will aid farmers in monitoring and managing crop growth and health, ultimately enhancing production efficiency. Conducting a cost-benefit analysis is also crucial to ensure the economic viability of this technology for farmers and the agricultural industry. Additionally, continuous technical support is necessary to ensure the system's stable operation, and compliance with relevant regulations is essential for technology sustainability.

Acknowledgements This work was supported by the National Natural Science Foundation of China (U20A2038, 22022404, 21977036, 22074050) and the CRI Project of National Research Foundation of Republic of Korea (2018R1A3B1052702). Amit Sharma thanks Department of Biotechnology, New Delhi, India, for prestigious DBT-Ramalingaswami fellowship (BT/RLF/Re-entry/59/2018) and Science & Engineering Research Board, New Delhi (CRG/2021/002476).

Conflict of interest The authors declare no conflict of interest.

1 Pawlak K, Kołodziejczak M. *Sustainability*, 2020, 12: 5488
2 Hunter MC, Smith RG, Schipanski ME, Atwood LW, Mortensen DA. *BioScience*, 2017, 67: 386–391
3 Tilman D, Balzer C, Hill J, Befort BL. *Proc Natl Acad Sci USA*, 2011, 108: 20260–20264
4 Zhou GH, Wang P, Yuan J, Qiu T, He ZK. *Sci China Chem*, 2011, 54: 1298–1303
5 Bokor B, Santos CS, Kostoláni D, Machado J, da Silva MN, Carvalho SMP, Vaculík M, Vasconcelos MW. *J Hazard Mater*, 2021, 416: 126193
6 Paul R, Saville AC, Hansel JC, Ye Y, Ball C, Williams A, Chang X, Chen G, Gu Z, Ristaino JB, Wei Q. *ACS Nano*, 2019, 13: 6540–6549
7 Farooq U, Yang Q, Ullah MW, Wang S. *Biosens Bioelectron*, 2018, 118: 204–216
8 Khater M, de la Escosura-Muñiz A, Merkoçi A. *Biosens Bioelectron*, 2017, 93: 72–86
9 Li Z, Yu T, Paul R, Fan J, Yang Y, Wei Q. *Nanoscale Adv*, 2020, 2: 3083–3094
10 Ali MM, Bachik NA, Muhadi N, Tuan Yusof TN, Gomes C. *Physiol Mol Plant Pathol*, 2019, 108: 101426
11 Qin J, Monje O, Nugent MR, Finn JR, O'Rourke AE, Wilson KD, Fritsche RF, Baek I, Chan DE, Kim MS. *Front Plant Sci*, 2023, 14: 1133505
12 Lowe A, Harrison N, French AP. *Plant Methods*, 2017, 13: 80
13 Mahlein AK. *Plant Dis*, 2016, 100: 241–251
14 Zhang N, Yang G, Pan Y, Yang X, Chen L, Zhao C. *Remote Sens*, 2020, 12: 3188
15 Zhou Y, Hua J, Tang BZ, Tang Y. *Sci China Chem*, 2019, 62: 1312–1332
16 Li B, Zhao M, Lin J, Huang P, Chen X. *Chem Soc Rev*, 2022, 51: 7692–7714
17 Zhang Z, Kang M, Tan H, Song N, Li M, Xiao P, Yan D, Zhang L, Wang D, Tang BZ. *Chem Soc Rev*, 2022, 51: 1983–2030
18 Wu M, Yin C, Jiang X, Sun Q, Xu X, Ma Y, Liu X, Niu N, Chen L. *Anal Chem*, 2022, 94: 8999–9008
19 Paper JM, Mukherjee T, Schrick K. *Plant Methods*, 2018, 14: 31
20 Carraretto L, Teardo E, Checchetto V, Finazzi G, Uozumi N, Szabo I. *Mol Plant*, 2016, 9: 371–395
21 Liu Y, Li Y, Koo S, Sun Y, Liu Y, Liu X, Pan Y, Zhang Z, Du M, Lu S, Qiao X, Gao J, Wang X, Deng Z, Meng X, Xiao Y, Kim JS, Hong X. *Chem Rev*, 2022, 122: 209–268
22 Xu Y, Dou Y, Li Q, Ye H, Li Y, Qiu S, Xiong X, Li J, Sun Y. *Coord Chem Rev*, 2023, 493: 215320
23 Li C, Pang Y, Xu Y, Lu M, Tu L, Li Q, Sharma A, Guo Z, Li X, Sun Y. *Chem Soc Rev*, 2023, 52: 4392–4442
24 Park MJ, Jung HS, Kim YJ, Kwon YJ, Lee JK, Park CM. *Chem Commun*, 2014, 50: 8547–8549
25 Fu YX, Liu SY, Guo WY, Dong J, Nan JX, Lin HY, Mei LC, Yang WC, Yang GF. *Plant Physiol*, 2022, 190: 196–201
26 Donaldson LA. *Plant Methods*, 2022, 18: 27
27 Polonio Á, Pineda M, Bautista R, Martínez-Cruz J, Pérez-Bueno ML, Barón M, Pérez-García A. *Sci Rep*, 2019, 9: 7978
28 Donaldson L. *Molecules*, 2020, 25: 2393
29 Zhang F, Wu X, Liu B, Han T, Yan D, Wang D, Zhong Tang B. *Coord Chem Rev*, 2023, 493: 215337
30 Sun Z, Shi S, Guan P, Liu B. *SpectroChim Acta Part A-Mol Biomol Spectr*, 2022, 272: 120946
31 Jia HR, Zhu YX, Xu KF, Pan GY, Liu X, Qiao Y, Wu FG. *Chem Sci*, 2019, 10: 4062–4068
32 Chen G, Zhang Y, Peng Z, Huang D, Li C, Wang Q. *Nano Res*, 2019, 12: 1321–1326
33 Wu MY, Leung JK, Kam C, Chou TY, Wang JL, Zhao X, Feng S, Chen S. *Sci China Chem*, 2022, 65: 979–988
34 Liu X, Xiang MH, Zhou WJ, Wang F, Chu X, Jiang JH. *Chem Sci*,

2021, 12: 5834–5842
35 Niu J, Ma Y, Yang Y, Lv H, Wang J, Wang T, Liu F, Xu S, Jiang Z, Lin W. *Coord Chem Rev*, 2023, 476: 214926
36 Luo J, Xie Z, Lam JWY, Cheng L, Tang BZ, Chen H, Qiu C, Kwok HS, Zhan X, Liu Y, Zhu D. *Chem Commun*, 2001, 1740–1741
37 Zuo J, Zhu E, Yin W, Yao C, Liao J, Ping X, Zhu Y, Cai X, Rao Y, Feng H, Zhang K, Qian Z. *Chem Sci*, 2023, 14: 2139–2148
38 Riahin C, Meares A, Esemoto NN, Ptaszek M, LaScola M, Pandala N, Lavik E, Yang M, Stacey G, Hu D, Traeger JC, Orr G, Rosenzweig Z. *ACS Appl Mater Interfaces*, 2022, 14: 20790–20801
39 Jia T, Chen G. *Coord Chem Rev*, 2022, 471: 214724
40 Xu J, Gulzar A, Yang P, Bi H, Yang D, Gai S, He F, Lin J, Xing B, Jin D. *Coord Chem Rev*, 2019, 381: 104–134
41 Jin GQ, Chau CV, Arambula JF, Gao S, Sessler JL, Zhang JL. *Chem Soc Rev*, 2022, 51: 6177–6209
42 Hischemöller A, Nordmann J, Ptacek P, Mummenhoff K, Haase M. *J BioMed Nanotechnol*, 2009, 5: 278–284
43 Wang J, Li C, Cui Y, Wang Q, Ye J, Yang J, Liu Z, Zhang S, Fu Y, Xu J. *Nanoscale*, 2023, 15: 11026–11037
44 Fu YX, Guo WY, Wang N, Dai YJ, Zhang ZY, Sun XL, Yang WC, Yang GF. *Anal Chem*, 2022, 94: 17692–17699
45 Jez JM, Lee SG, Sherp AM. *Science*, 2016, 353: 1241–1244
46 Zhu JK. *Cell*, 2016, 167: 313–324
47 Savvides A, Ali S, Tester M, Fotopoulos V. *Trends Plant Sci*, 2016, 21: 329–340
48 Waszczak C, Carmody M, Kangasjärvi J. *Annu Rev Plant Biol*, 2018, 69: 209–236
49 Qi WY, Li Q, Chen H, Liu J, Xing SF, Xu M, Yan Z, Song C, Wang SG. *J Hazard Mater*, 2021, 417: 125900
50 Zhang Y, Fu L, Jeon S, Yan J, Giraldo JP, Matyjaszewski K, Tilton RD, Lowry GV. *ACS Nano*, 2022, 16: 4467–4478
51 Cheng M, Wang L, Zhou Q, Chao D, Nagawa S, He D, Zhang J, Li H, Tan L, Gu Z, Huang X, Yang Z. *Nat Commun*, 2021, 12: 4327
52 Zeng X, Chen W, Liu C, Yin J, Yang GF. *J Agric Food Chem*, 2021, 69: 13700–13712
53 Aroca A, Yruela I, Gotor C, Bassham DC. *Proc Natl Acad Sci USA*, 2021, 118: e2023604118
54 Jiang G, Li M, Wen Y, Zeng W, Zhao Q, Chen C, Yuan H, Liu C, Liu C. *ACS Sens*, 2019, 4: 434–440
55 Zhang J, Zhou M, Zhou H, Zhao D, Gotor C, Romero LC, Shen J, Ge Z, Zhang Z, Shen W, Yuan X, Xie Y. *JIPB*, 2021, 63: 146–160
56 Liang K, Li Y, Zeng F, Wu S. *New J Chem*, 2023, 47: 2643–2650
57 Lin YM, He Q, Wang XY, Hua FF, Liu XY, Fu YL. *J Agric Food Chem*, 2023, 71: 5154–5161
58 Wang J, Xie H, Li H, Wang R, Zhang B, Ren T, Hua J, Chen N. *J Agric Food Chem*, 2021, 69: 14330–14339
59 Shi W, Wang L, Yao L, Hao W, Han C, Fan M, Wang W, Bai MY. *Nat Commun*, 2022, 13: 5040
60 Su T, Wang P, Li H, Zhao Y, Lu Y, Dai P, Ren T, Wang X, Li X, Shao Q, Zhao D, Zhao Y, Ma C. *JIPB*, 2018, 60: 591–607
61 Wu F, Chi Y, Jiang Z, Xu Y, Xie L, Huang F, Wan D, Ni J, Yuan F, Wu X, Zhang Y, Wang L, Ye R, Byeon B, Wang W, Zhang S, Sima M, Chen S, Zhu M, Pei J, Johnson DM, Zhu S, Cao X, Pei C, Zai Z, Liu Y, Liu T, Swift GB, Zhang W, Yu M, Hu Z, Siedow JN, Chen X, Pei ZM. *Nature*, 2020, 578: 577–581
62 Zeng C, Long Y, Tan Y, Zeng F, Wu S. *Anal Chem*, 2022, 94: 14021–14028
63 Long Y, Chen J, Zeng F, Wu S. *Aggregate*, 2023, 4: e288
64 Welsher K, Liu Z, Sherlock SP, Robinson JT, Chen Z, Daranciang D, Dai H. *Nat Nanotech*, 2009, 4: 773–780
65 Wu H, Nißler R, Morris V, Herrmann N, Hu P, Jeon SJ, Kruss S, Giraldo JP. *Nano Lett*, 2020, 20: 2432–2442
66 Santner A, Estelle M. *Nature*, 2009, 459: 1071–1078
67 Cao M, Chen R, Li P, Yu Y, Zheng R, Ge D, Zheng W, Wang X, Gu Y, Gelová Z, Friml J, Zhang H, Liu R, He J, Xu T. *Nature*, 2019, 568: 240–243
68 Ang MCY, Dhar N, Khong DT, Lew TTS, Park M, Sarangapani S, Cui J, Dehadrai A, Singh GP, Chan-Park MB, Sarojam R, Strano M. *ACS Sens*, 2021, 6: 3032–3046
69 Boonyaves K, Ang MCY, Park M, Cui J, Khong DT, Singh GP, Koman VB, Gong X, Porter TK, Choi SW, Chung K, Chua NH, Urano D, Strano MS. *Nano Lett*, 2023, 23: 916–924
70 Chen J, Chen L, Fang Y, Zeng F, Wu S. *Cell Rep Phys Sci*, 2022, 3: 100570
71 Yang X, Zhang Q, Zhang S, Lai M, Ji X, Ye Y, Li H, Zhao M. *Coord Chem Rev*, 2023, 487: 215154
72 Du J, Chen K, Yu Z, Qiao Y, Liu J, Zhai Q, Hu Z, Yang SG, Li J, Teng H. *Adv Agrochem*, 2022, 1: 162–173
73 Li H, Kim H, Xu F, Han J, Yao Q, Wang J, Pu K, Peng X, Yoon J. *Chem Soc Rev*, 2022, 51: 1795–1835
74 Zhao X, Zhang F, Lei Z. *Chem Sci*, 2022, 13: 11280–11293
75 Wang S, Ren WX, Hou JT, Won M, An J, Chen X, Shu J, Kim JS. *Chem Soc Rev*, 2021, 50: 8887–8902
76 Zeng L, Ma G, Xu H, Mu J, Li F, Gao X, Deng Z, Qu J, Huang P, Lin J. *Small*, 2019, 15: 1803866
77 Chen W, Guan Y, Chen Q, Ren J, Xie Y, Yin J. *Dyes Pigments*, 2022, 200: 110134
78 Lee MA, Wang S, Jin X, Bakh NA, Nguyen FT, Dong J, Silmore KS, Gong X, Pham C, Jones KK, Muthupalani S, Bisker G, Son M, Strano MS. *Adv Healthc Mater*, 2020, 9: 2000429
79 Lew TTS, Park M, Cui J, Strano MS. *Adv Mater*, 2021, 33: 2005683
80 Wang L, Ma Y, Yin J, Zhu L, Li S, Lin W. *Sens Actuat B-Chem*, 2022, 358: 131508
81 Deng G, Li S, Sun Z, Li W, Zhou L, Zhang J, Gong P, Cai L. *Theranostics*, 2018, 8: 4116–4128
82 Long L, Han Y, Yuan X, Cao S, Liu W, Chen Q, Wang K, Han Z. *Food Chem*, 2020, 331: 127359
83 Tavakkoli E, Rengasamy P, McDonald GK. *J Exp Bot*, 2010, 61: 4449–4459
84 Yu Z, Duan X, Luo L, Dai S, Ding Z, Xia G. *Trends Plant Sci*, 2020, 25: 1117–1130
85 Chrysargyris A, Papakyriakou E, Petropoulos SA, Tzortzakis N. *J Hazard Mater*, 2019, 368: 584–593
86 Ma X, Huang Y, Chen W, Liu J, Liu SH, Yin J, Yang GF. *Angew Chem Int Ed*, 2023, 62: e202216109
87 Yan L, Zhang S, Xie Y, Mu X, Zhu J. *Crit Rev Anal Chem*, 2022, 52: 210–229
88 Lai Q, Si S, Qin T, Li B, Wu H, Liu B, Xu H, Zhao C. *Sens Actuat B-Chem*, 2020, 307: 127640
89 Oguz M, Erdemir S, Malkondu S. *Anal Chim Acta*, 2022, 1227: 340320
90 Li Z, Xu Y, Zhu H, Qian Y. *Chem Sci*, 2017, 8: 5616–5621
91 Peng WX, Yue X, Chen H, Ma NL, Quan Z, Yu Q, Wei Z, Guan R, Lam SS, Rinklebe J, Zhang D, Zhang B, Bolan N, Kirkham MB, Sonne C. *J Hazard Mater*, 2022, 436: 129304
92 Min Z, Zhang M, Sun H, Xu L, Wang X, Liu Z. *Dyes Pigments*, 2023, 218: 111446
93 Gao G, Wang J, Wang X, Liu G, Fan L, Ru G, Wang S, Song M, Shen W, Zheng X, Han L, Liu L. *Anal Chem*, 2022, 94: 13590–13597
94 Deng G, Cheung FMH, Sun Z, Peng X, Li S, Gong P, Cai L. *Chem Commun*, 2018, 54: 13240–13243
95 Rolfe SA, Scholes JD. *Protoplasma*, 2010, 247: 163–175
96 Feng X, Yu C, Chen Y, Peng J, Ye L, Shen T, Wen H, He Y. *Front Plant Sci*, 2018, 9: 468
97 Rananaware A, Bhosale RS, Ohkubo K, Patil H, Jones LA, Jackson SL, Fukuzumi S, Bhosale SV, Bhosale SV. *J Org Chem*, 2015, 80: 3832–3840
98 Ivanov DA, Bernards MA. *Planta*, 2016, 243: 263–279
99 Xu Y, Li C, Ma X, Tuo W, Tu L, Li X, Sun Y, Stang PJ, Sun Y. *Proc Natl Acad Sci USA*, 2022, 119: e2209904119
100 Li C, Tu L, Yang J, Liu C, Xu Y, Li J, Tuo W, Olenyuk B, Sun Y, Stang PJ, Sun Y. *Chem Sci*, 2023, 14: 2901–2909
101 He S, Song J, Qu J, Cheng Z. *Chem Soc Rev*, 2018, 47: 4258–4278

102 Li C, Guan X, Zhang X, Zhou D, Son S, Xu Y, Deng M, Guo Z, Sun Y, Kim JS. *Biosens Bioelectron*, 2022, 216: 114620
103 Tu L, Li C, Xiong X, Hyeon Kim J, Li Q, Mei L, Li J, Liu S, Seung Kim J, Sun Y. *Angew Chem Int Ed*, 2023, 62: e202301560
104 Sun M, Müllen K, Yin M. *Chem Soc Rev*, 2016, 45: 1513–1528
105 Tang X, Li A, Zuo C, Liu X, Luo X, Chen L, Li L, Lin H, Gao J. *ACS Nano*, 2023, 17: 5014–5024
106 Yanai H, Hoshikawa S, Moriiwa Y, Shoji A, Yanagida A, Matsumoto T. *Angew Chem Int Ed*, 2021, 60: 5168–5172
107 Jet T, Gines G, Rondelez Y, Taly V. *Chem Soc Rev*, 2021, 50: 4141–4161
108 Laing S, Gracie K, Faulds K. *Chem Soc Rev*, 2016, 45: 1901–1918
109 Castro RC, Saraiva MLMFS, Santos JLM, Ribeiro DSM. *Coord Chem Rev*, 2021, 448: 214181
110 Xu S, Ma W, Bai Y, Liu H. *J Am Chem Soc*, 2019, 141: 72–75
111 Cheng HB, Li Y, Tang BZ, Yoon J. *Chem Soc Rev*, 2020, 49: 21–31
112 Weng S, Hu X, Wang J, Tang L, Li P, Zheng S, Zheng L, Huang L, Xin Z. *J Agric Food Chem*, 2021, 69: 2950–2964
113 Son WK, Choi YS, Han YW, Shin DW, Min K, Shin J, Lee MJ, Son H, Jeong DH, Kwak SY. *Nat Nanotechnol*, 2023, 18: 205–216
114 Gan Q, Wang X, Wang Y, Xie Z, Tian Y, Lu Y. *Adv Sci*, 2017, 4: 1700127
115 Zhang Z, Guan R, Li J, Sun Y. *Chemosensors*, 2023, 11: 110
116 Wen L, Cao Y, Cheng Q, Li X, Pan L, Li L, Zhu H, Lan W, Yang Z. *Br J Ophthalmol*, 2020, 104: 1542–1547